10.24425/acs.2025.153956

Archives of Control Sciences
Volume 35(LXXI), 2025
No. 1, *pages 1–17*

Sliding Mode Controller navigation algorithm using tag-based fiducial marker detection and fuzzy logic system

Mohammad Soleimani AMIRI, Rizauddin RAMLI and Ahmad BARARI

Autonomous navigation of vehicles, especially drones, plays an essential role in Industrial Revolution 4.0. Maneuvering drone in complex path especially indoor environment requires stable and accurate navigation system. This paper investigates a navigation algorithm for maneuvering a drone by Sliding Mode Controller (SMC) combined by fuzzy logic system, model reference approach, and tag-based fiducial marker detection in an indoor environment. The SMC parameters are tuned by the fuzzy logic system and model reference approach. A drone model is simulated in a virtual indoor environment to validate the performance of the navigation system with different home points and trajectories. The desired set-points of the control system are obtained by AprilTag, which is a tag-based fiducial marker detection system. The stability of the SMC was verified using the Lyapunov stability theory. The performance of proposed SMC navigation algorithm validated by comparing to conventional controllers which represents the effectiveness of SMC. It can be ascertained that the proposed SMC navigation algorithm is applicable to maneuver the drone for various industrial tasks in indoor environment.

Key words: fuzzy logic, sliding mode controller, autonomous navigation, fiducial marker detection

M.S. Amiri (corresponding author, e-mail: soleimani@utem.edu.my) is with Department of Manufacturing Engineering Technology, Faculty of Industrial and Manufacturing Technology and Engineering, Universiti Teknikal Malaysia Melaka, 76100 Durian Tunggal, Melaka, Malaysia.

R. Ramli is with Department of Mechanical and Manufacturing Engineering, Faculty of Engineering and Built Environment, Universiti Kebangsaan Malaysia, 43600 Bangi, Selangor, Malaysia.

A. Barari is with Advanced Digital Design and Manufacturing and Advanced Digital Metrology Laboratories (AD2M Labs), Department of Mechanical and Manufacturing Engineering, University of Ontario Institute of Technology, Oshawa, Ontario, L1H7K4, Canada.

The authors would like to thank the Universiti Teknikal Malaysia Melaka (UTeM) for the financial support received under grant scheme PJP/2024/FTKIP/PERINTIS/SA0022.

Received 7.02.2024. Revised 17.01.2025.

1. Introduction

Unmanned Aerial Vehicles or drones have been used in industries due to their efficiencies in aerial photography and ability to access hazardous places in various civilian and military applications [1,2]. Precise navigation of autonomous drones scheme in disturbed environments has been developed in several works [3, 4]. Selma et al. [5] presented a novel tracking hybrid controller for a quadrotor drone that combined a robust adaptive neuro-fuzzy inference system and particle swarm optimization algorithm for navigation. In some works, Proportional-Integral-Derivative (PID) is employed to navigate the drone in a specific trajectory [6, 7]. Babu et al. [8] utilized a gradient descent-based self-tuning PID controller for flight control of an Augmented Reality (AR) drone. Similarly, Merheb et al. [9] established a fault-tolerant PID-based controller for an AR drone in emergency cases such as suffering damage to one actuator.

The fiducial marker detection system is an accurate technique to obtain the position and orientation of a certain tag relative to camera [10, 11]. Because of the affordability, accessibility, and accuracy of the marker detection technique, the tag has been used in drone applications recently. For example, Kawabata et al. [12] developed an obstacle avoidance algorithm based on visual navigation to obtain the position information of the drone in indoor environments without Global Positioning System (GPS) information. Malyuta et al. [13] utilized an autonomous drone for precision agriculture applications. They employed the drone for long-term monitoring missions without any human supervision through the farmland by using AprilTag. Tang et al. [14] developed an algorithm powered by a multi-sensor system including multiple cameras and a 2-D laser scanner using the AprilTag array as the calibration target for drone application.

Developing an efficient control strategy has attracted much attention from researchers. The classical control systems are largely utilized in the generality of control systems [15]. In a complex mathematical model, this approach does not conclude satisfactory performance [16]. Therefore, fuzzy logic has been used for the real-time tuning of controller parameters in various works [17]. For instance, Navabi et al. [18] studied quaternion-based fuzzy gain scheduling Proportional-Derivative (PD) controller. Similarly, Salabun et al. [19] investigated a Proportional-Integral-Derivative (PID) controller online tuning by fuzzy logic for a multi-input single-output crane relocating container with the external distribution. Shi et al. [20] proposed a fractional-order Fuzzy-PID controller for a practical inverted pendulum system, that improved the speed, acceleration response, and stability time in comparing conventional PID control systems. Han et al. [21] proposed an adaptive fuzzy control strategy integrated with barrier Lyapunov function including event-triggered mechanism and spatial motion constraint for a hybrid spacecraft system.

From literature [15–21], there are several types of controller strategies to improve controller's performance for nonlinear systems. The fuzzy logic system and model reference approach are used to minimize the complexity of computation and reduce processing time and computational burden. This paper presents an Adaptive Sliding Mode Controller (SMC) integrated with fuzzy logic system and model reference approach for precise navigation of a drone based on fiducial marker detection. In general, the contributions of this paper are as follows:

- The investigation of SMC for drone navigation.
- The determination of SMC parameters by fuzzy logic system and model reference approach in real-time.
- The utilization of AprilTag as a tag-based fiducial marker detection system to set desired set-points for the control system.

The structure of this paper is outlined as follows: dynamic models of a drone are presented in Section 2. Section 3 delves into the development of SMC and discusses the stability of the control system. Stability analysis of SMC is detailed in Section 4. Section 5 represents the performance and results of the proposed SMC strategy in real-time navigation of a drone model within a virtual environment integrated with the Robot Operating System (ROS). The conclusion can be found in Section 6.

2. Dynamic model

To analyze the system modeling including dynamic and motion equations, the drone earth $\{E\}$ and body $\{B\}$ reference frames are introduced. The earth frame reference is a fixed frame located in the ground. The body reference frame is located at the center of mass and its axes are aligned with the sensor for reading the altitude data. The equation of dynamic, developed by external forces applied to a rigid body is given as follows [22]:

$$M\dot{V}^B + \omega \times MV^B = F^B, \tag{1}$$

$$I\dot{\omega}^B + \omega \times I\omega^B = \mu^B, \tag{2}$$

here M and $I \in \Re^{3\times3}$ are the mass and inertia matrices, $V^B = \begin{bmatrix}\dot{x} & \dot{y} & \dot{z}\end{bmatrix}^T$ (m/s) and $\omega^B = \begin{bmatrix}\dot{\psi} & \dot{\theta} & \dot{\phi}\end{bmatrix}^T$ (rad/s) are linear and angular velocity vectors in the body frame. Similarly, $\dot{V}^B$ and $\dot{\omega}^B$ represent linear and angular acceleration vectors in body frame. μ^B is the torque that applies at the drone's center of gravity. F^B is forces applied to the drone as

$$F^B = F_t^B + F_d^B + F_a^B + F_g^B, \tag{3}$$

where F_t^B is the trust force that uplifts the drone and it is determined by the summation of the angular velocity of the propellers. F_d^B is the drag force acting on the body of the drone in X-axis and Y-axis. F_a^B is the air resistance force proportion to the squared linear velocity of the body. F_g^B is the gravitational force in Z-axis. These forces are represented as follows:

$$F_t^B = b \cdot \sum_{i=1}^{n} \Omega_i^2 e_3 \,, \tag{4}$$

$$F_d^B = -C_d \times V^B, \tag{5}$$

$$F_a^B = -\frac{1}{2} C_a A \rho V^{B2}, \tag{6}$$

$$F_g^B = -g R_E^B M e_3, \tag{7}$$

where b (N·s^2) is the trust constant for actuators of the drone. Ω_i is the angular velocity of each propeller and n is the number of propellers. $e_3 = \begin{bmatrix} 0 & 0 & 1 \end{bmatrix}^T$ is the basis vector that expresses the downward direction of drone. C_d represents the drag constant. C_a and ρ (kg/m^3) are dimensionless friction constant and the density of air. A (m^2) $\in \Re^{3\times3}$ is the cross-sectional area matrix of the drone. Therefore, the state vector is represented as follows:

$$\eta = \begin{bmatrix} x & y & z & \phi \end{bmatrix}^T . \tag{8}$$

3. Development of SMC for drone navigation

SMC is a robust non-linear control strategy designed to manage uncertainties and disturbances in dynamic systems which has been derived based on variable structure control. he main objective of SMC consists of two key elements i.e. initially, it involves formulating a control law to guide the error vector towards a predefined decision rule, referred to as the sliding surface, during the reaching phase. In this phase, the control switches across various sides of the sliding surface. Subsequently, once the error vector is constrained within the sliding surface, the controller follows the dynamics dictated by the equations characterizing the sliding surface. This latter part of the controller is denoted as equivalent control.

In this paper, a SMC for navigation of drone in indoor environment is determined by setting a desired set-points of the control system that can be obtained by using AprilTag. The feedback control is adjusted based on the difference between the actual and desired drone position, orientation, and targeted values obtained from AprilTag. The control system is divided into three stages: SMC, which is the control law, fuzzy logic system and model reference approach, that are utilized to

tune the parameters of SMC. The drone's motion in the forward, backward, left, right, upward, or downward directions is controlled by the SMC's output signals. Figure 1 shows the block diagram of the SMC strategies.

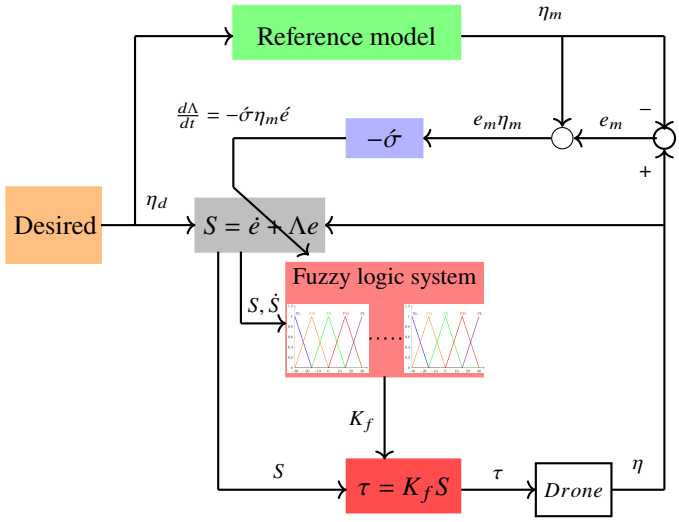

Figure 1: Block diagram of SMC integrated with fuzzy logic system and model reference approach

The control law for SMC is given as follows:

$$\tau = K_f S, \tag{9}$$

where τ is the output of the controller. K_f is the controller parameter and S represents the sliding filtered steady-state error given by:

$$S = \dot{e} + \Lambda e, \tag{10}$$

where $\Lambda \in \Re^{4\times4}$ is the symmetric positive constant gain matrix; e and $\dot{e}$ are steady-state error and its derivative as follows:

$$e = \eta_d - \eta, \tag{11}$$

where $e = \begin{bmatrix} e_x & e_y & e_z & e_\phi \end{bmatrix}^T$ is the error vector; $\eta_d = \begin{bmatrix} x_d & y_d & z_d & \phi_d \end{bmatrix}^T$ is desired vector. The controller parameters K_f and Λ are determined in real-time by fuzzy logic system and model reference approach respectively.

3.1. Fuzzy logic system

Fuzzy logic consists of three main parts including fuzzification, fuzzy inference, and defuzzification [23].

• Fuzzification

Fuzzification serves as the input for the fuzzy control system, generating a fuzzy quantity through the transformation of membership sets for fuzzy inference. If we designate A as a fuzzy set, the membership function can be defined as follows:

$$A = \{x, \mu(x) | \forall x \in X, \mu(x) \in [0, 1]\}, \tag{12}$$

where X is the universal base set. α is the subset of set A, which is represented by:

$$A_\alpha = \{x, |\mu(x) \geqslant \alpha, \ \alpha \in [0, 1]\}. \tag{13}$$

Several typical membership functions, such as triangular, trapezoidal, and Gaussian, exhibit distinct shapes in their graphs. In such instances, where the sensitivity of the membership function to shape variations is not crucial, simpler membership functions prove to be convenient.

• Fuzzy Inference Machine

The fuzzy inference machine combines the data derived from fuzzification with the specified linguistic IF-THEN rules. Serving as the core of fuzzy logic, fuzzy inference processes the input antecedent through linguistic rules and deduces the corresponding output consequently.

• Defuzzification

Defuzzification is the procedure of transforming the linguistic outcomes of fuzzy inference into tangible, meaningful crisp values, representing the output of the fuzzy logic control. This conversion can be accomplished through different methods, including the center of gravity, weighted average, center of the largest area, and centroid methods.

The real-time determination of K_f is achieved through fuzzy rules. Fuzzification's membership function is constructed based on the sliding filtered steady-state error and its derivative, denoted as S and $\dot{S}$. Additionally, a set of membership functions is defined for defuzzification. Consequently, fuzzy inference involves two inputs, namely S and $\dot{S}$, and one output, which is K_f. The subsets for fuzzification membership functions are Negative Large (NL), Negative Medium (NM), Zero (ZE), Positive Medium (PM), and Positive Large (PL) [24]. Similarly, subsets for defuzzification membership functions are ZE, PS, PM, PB, and PL. In Table 1, the linguistic rules for K_f are outlined.

The fuzzy logic rules are defined as follows:

$$\text{if} \quad s_i = L_i \quad \& \quad \dot{s} = H_i \quad \text{then} \quad K_f = T_i \,. \tag{14}$$

In this context, L_i and H_i denote labels for input fuzzy subsets, while T_i represents output fuzzy subsets. Specifically, two examples of fuzzy logic rules are

Table 1: Fuzzy logic rules for K_f

S \ $\dot{S}$	NL	NM	ZE	PM	PL
NL	PL	PL	ZE	PS	PS
NM	PL	PB	ZE	PS	PS
ZE	PB	PM	ZE	PM	PM
PM	PM	PM	PS	PB	PL
PL	PL	PS	PS	PB	PL

formulated as follows:

$$\text{if} \quad s_i = NL \quad \& \quad \dot{s} = ZE \quad \text{then} \quad K_f = ZE, \tag{15}$$

$$\text{if} \quad s_i = PM \quad \& \quad \dot{s} = NM \quad \text{then} \quad K_f = PM. \tag{16}$$

In defuzzification center of gravity technique and Zadeh fuzzy synthesis method are used [25].

3.2. Model reference approach

Model reference approach, which is a gradient-based optimization method, is utilized to improve the performance of SMC. It determines the tracking error $\acute{e}$ by comparing a reference model to the actual drone position and orientation states. It tunes Λ by minimizing the tracking error to zero in real-time. Therefore, $\frac{\mathrm{d}\Lambda}{\mathrm{d}t}$ is established based on the tracking error $\acute{e}$, which is the difference between the actual position and orientation state η, and the reference model η_m.

$$\acute{e} = \eta - \eta_m. \tag{17}$$

Thus, the following cost function is minimized:

$$J(\Lambda) = \frac{1}{2}\acute{e}_m^2 \,. \tag{18}$$

The changes in Λ a in the direction of the negative gradient of J is given by:

$$\frac{\mathrm{d}\Lambda}{\mathrm{d}t} = -\sigma\frac{\partial J}{\partial \Lambda} = -\sigma\frac{\partial J}{\partial \acute{e}}\frac{\partial \acute{e}}{\partial \Lambda} \,. \tag{19}$$

The negative sign indicates that Λ undergoes changes to minimize J, where $\frac{\partial \acute{e}}{\partial \Lambda}$ represents the sensitivity derivatives of the tracking error. The symbol σ

denotes the speed of adaptation. Therefore,

$$\frac{\partial J}{\partial \acute{e}} = \acute{e}. \tag{20}$$

Thus, equation (19) is rewritten as follows:

$$\frac{\mathrm{d}\Lambda}{\mathrm{d}t} = -\sigma \acute{e} \frac{\partial \acute{e}}{\partial \Lambda}. \tag{21}$$

The schematic of the drone model in the frequency domain is represented by:

$$\frac{\eta}{\tau} = KG(s), \tag{22}$$

where K is an unknown gain and $G(s)$ is the transfer function of drone model in frequency domain. The model reference is given as follows:

$$\frac{\eta_m}{\eta_d} = K_0 G(s), \tag{23}$$

where K_0 is a constant. Sensitivity derivatives of tracking error is given by:

$$\frac{\partial \acute{e}}{\partial \Lambda} = KG(s)\eta_d. \tag{24}$$

Consequently, equation (21) is reconsidered as:

$$\frac{\mathrm{d}\Lambda}{\mathrm{d}t} = -\sigma \acute{e} KG(s)\eta_d. \tag{25}$$

However, $G(s)\eta_d$ cannot be obtained directly, thus, rearrangement of equation (23) is derived,

$$G(s)\eta_d = \frac{\eta_m}{K_0}. \tag{26}$$

Therefore,

$$\frac{\mathrm{d}\Lambda}{\mathrm{d}t} = -\sigma \acute{e} \frac{K}{K_0}\eta_m. \tag{27}$$

We define $\acute{\sigma} = \sigma \dfrac{K}{K_0}$. Thus,

$$\frac{\mathrm{d}\Lambda}{\mathrm{d}t} = -\acute{\sigma} \acute{e} \eta_m. \tag{28}$$

Equation (28) represents the adjustment of controller parameter Λ over time.

4. Stability analysis

The stability of the system using the proposed SMC is examined through the Lyapunov stability theory. Let's consider the general dynamic equation as follows:

$$\tau = M\ddot{\eta} + C(\dot{\eta}, \eta)\dot{\eta}. \tag{29}$$

Let's assume that η_d is constant in equation (11). Therefore,

$$\dot{e} = -\dot{\eta}, \quad \ddot{e} = -\ddot{\eta}. \tag{30}$$

Thus equation (29) is rewritten as follows:

$$\tau = -M\ddot{e} - C\dot{e}, \tag{31}$$

$$\ddot{e} = M^{-1}\tau + M^{-1}C\dot{e}. \tag{32}$$

Equation (10) is rewritten by:

$$S = D\begin{bmatrix} e \\ \dot{e} \end{bmatrix}, \tag{33}$$

where D is given as follows:

$$D = \begin{bmatrix} \Lambda I & 0 \\ 0 \end{bmatrix}, \tag{34}$$

where Λ is a positive constant matrix, $I \in \Re^{4\times4}$ is a identity matrix. Equation (33) in state space is described as follows:

$$\dot{S} = D\begin{bmatrix} \dot{e} \\ \ddot{e} \end{bmatrix}, \tag{35}$$

$$\dot{S} = D\begin{bmatrix} \dot{e} \\ M^{-1}\tau + M^{-1}C\dot{e} \end{bmatrix}, \tag{36}$$

$$\dot{S} = D\begin{bmatrix} 0 & I \\ 0 & M^{-1}C \end{bmatrix}\begin{bmatrix} e \\ \dot{e} \end{bmatrix} + D\begin{bmatrix} 0 \\ M^{-1} \end{bmatrix}\tau, \tag{37}$$

$$\dot{S} = D\begin{bmatrix} 0 & I \\ 0 & M^{-1}C \end{bmatrix}D^{-1}S + D\begin{bmatrix} 0 \\ M^{-1} \end{bmatrix}\tau, \tag{38}$$

$$\dot{S} = AS + B\tau, \tag{39}$$

where

$$A = D\begin{bmatrix} 0 & I \\ 0 & M^{-1}C \end{bmatrix}D^{-1}, \quad B = D\begin{bmatrix} 0 \\ M^{-1} \end{bmatrix}. \tag{40}$$

If a positive definite matrix $P \in \Re^{8\times 8}$ exists, the following equation is satisfied,

$$A^T P + PA = -Q, \tag{41}$$

where $Q \in \Re^{8\times 8}$ is a positive definite symmetric matrix. Then a positive-definite Lyapunov function candidate is chosen as follows:

$$V = \frac{1}{2} S^T P S. \tag{42}$$

Integrating equations (40), (41), and (42) yields

$$\dot{V} = \frac{1}{2}\dot{S}^T P S + \frac{1}{2} S^T P \dot{S}, \tag{43}$$

$$\dot{V} = \frac{1}{2}\left(S^T A^T + \tau^T B^T\right) P S + \frac{1}{2} S^T P (AS + B\tau), \tag{44}$$

$$\dot{V} = \frac{1}{2}\left(S^T A^T P S + \tau^T B^T P S + S^T P A S + S^T P B \tau\right), \tag{45}$$

$$\dot{V} = -\frac{1}{2} S^T Q S + \frac{1}{2}\tau^T B^T P S + \frac{1}{2} S^T P B \tau. \tag{46}$$

Therefore,

$$\dot{V} \leqslant \frac{1}{2}\tau^T B^T P S + \frac{1}{2} S^T P B \tau. \tag{47}$$

The controller output determined by SMC is constrained within a bound, specifically $|\tau| \leqslant \sigma$, where σ is a positive constant. Matrices B and P are assumed to be positive definite. The variable S depends on the steady-state error e and its derivative $\dot{e}$. As time approaches infinity ($t \to \infty$), the steady-state error diminishes ($e \to 0$), and its derivative becomes negative ($\dot{e} < 0$). Consequently, $S < 0$. Therefore, we have:

$$\frac{1}{2}\tau^T B^T P S + \frac{1}{2} S^T P B \tau < \gamma. \tag{48}$$

In this context, where γ is a positive constant, it is deduced that $\dot{V} < \gamma$, indicating that the rate of change of a certain variable is bounded within a specific range. This result serves as proof of the asymptotic stability of the control system.

5. Results and discussion

The performance of SMC navigation algorithm is validated for hovering experiment. To assess the navigation system, a drone model is constructed within a virtual environment called Gazebo, integrated with ROS [26–28]. In this environment, the actual parameters of gravitational force, aerodynamic factors, and

propellers are simulated. The tag marker is attached to a vertical bar and the drone flew from the home point to the front of the target. A camera is attached to the drone body to capture the tag data. In this experiment, The AprilTag integrated with ROS is employed to obtain the position of the drone regarding the tag marker located at the target point.

The navigation system is programmed in Python and runs in the base station, which is a PC with an Intel Core i3 CPU and 16 GB RAM. Table 2 expresses the parameters of the virtual environment and the drone.

Table 2: Parameters of the virtual environment and the drone

Parameters	Symbols (unit)	Values
Gravitational acceleration	g (m/s^2)	9.81
Mass of drone	M (kg)	4
Inertia	I_{xx} (Kgm^2)	0.01152
Inertia	I_{yy} (Kgm^2)	0.01152
Inertia	I_{zz} (Kgm^2)	0.0218
Trust constant	b (Ns^2)	0.013
Density of air	ρ (kg/m^3)	1.225
Drag constant	α	0.05
Dimensionless friction constant	C_a	0.07

Three different home points are defined to validate the performance of the navigation system with different home points and trajectories. Figure 2 shows the drone's body frame trajectories related to the earth frame in the virtual environment model, while the tolerance for lengths is 0.1 m and ϕ is 10°.

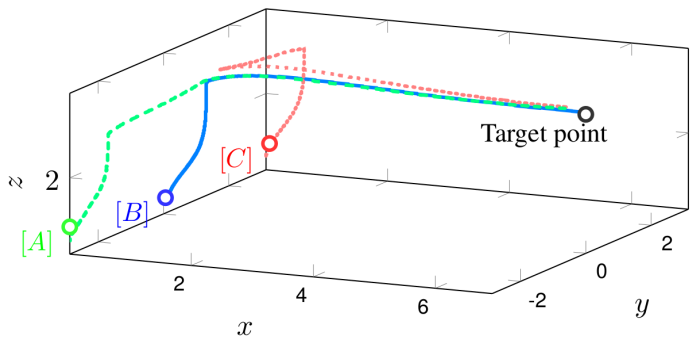

Figure 2: Drone trajectories in 3D using proposed tag-based navigation algorithm with different home points

Drone took off from three different home points, $A = [0, -3, 0, 0°]$, $B = [0, 0, 0, 0°]$, and $C = [0, 3, 0, 0°]$, toward the target point located in front of tag marker. Firstly the drone took off and moved in the y-direction of the body frame to adjust itself to the front of the tag marker then it moved in the x-direction of the body frame to hover in front of the tag marker. Figure 3 represents the comparison of SMC, Fuzzy Logic Controller (FLC), and conventional PID controller with constant parameters.

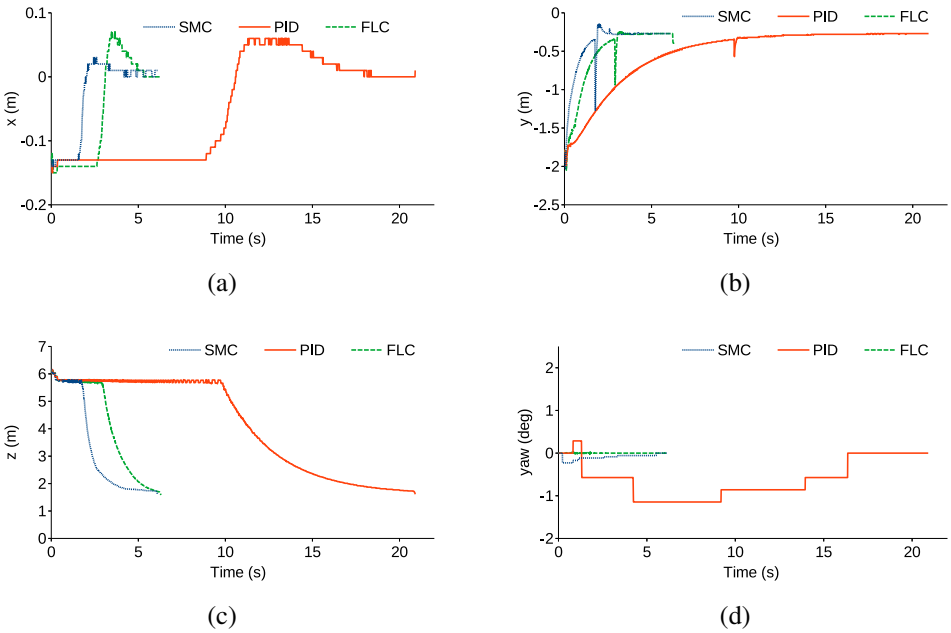

Figure 3: Comparison of SMC, FLC, and PID performance: X-axis of tag frame (a), Y-axis of tag frame (b), Z-axis of tag frame (c), ϕ of the tag frame (d)

In Figure 3, the navigation system with SMC converged faster to the desired points. The performance of the FLC is more efficient than the PID controller. It shows the superiority of the fuzzy controller over the conventional PID controller for the navigation system. The controller's parameters are tuned based on the fuzzy rules in real time. Therefore, it showed faster response and convergence and the drone reached the target point faster. Figure 3d) shows the drone is kept in front of the AprilTag marker for PID and SMC, although the angular trajectory target is passed faster. Figure 4 represents the changes in Λ while the drone was moving forward to the target point.

Figure 5 represents the changes in K_f, S, and $\dot{S}$, while the drone was moving forward to the target point to demonstrate the variation of K_f based on ranges of S and $\dot{S}$ by rules of the fuzzy logic system.

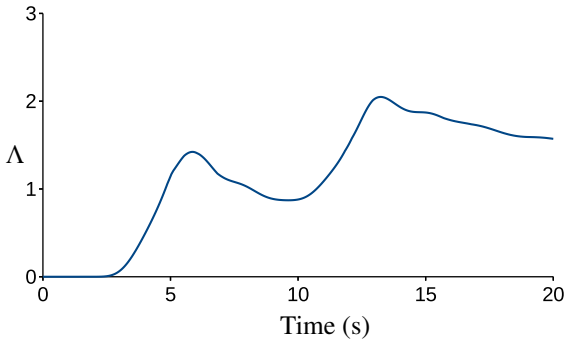

Figure 4: Changes of Λ, determined by model reference approach during the navigation

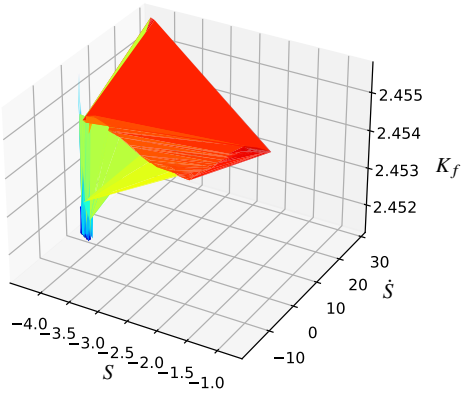

Figure 5: 3-Dimensional illustration of K_f over S and $\dot{S}$, determined by fuzzy logic system

In Figure 5, the K_f is adjusted in real-time over the changes of the S and $\dot{S}$ by rules of the fuzzy logic system. When the drone is located far from the target, the SMC parameters obtained the greatest value. While it reaches closer to the target, the controller parameters varied to move the drone slower to the target. Figure 6 illustrates the velocity of the drone while it is moving forward to the tag marker.

The velocity decreased while the drone is reaching closer to the target. Three different home points are defined to validate the performance of the navigation system with different home points and trajectories. Figure 7 represents the convergence of trajectory error in x, y, z, and ϕ.

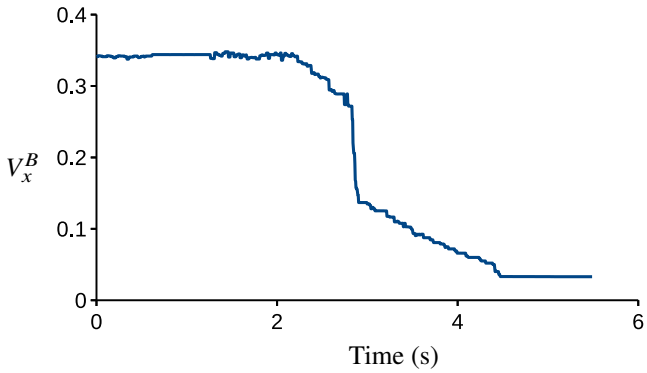

Figure 6: Velocity of the drone moving forward to the tag marker

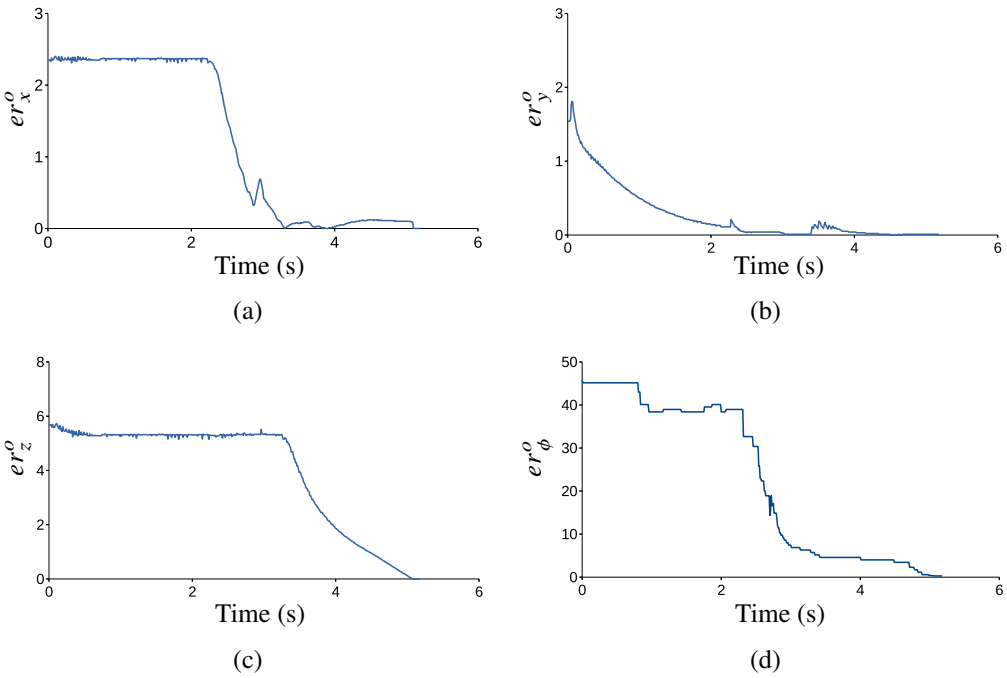

Figure 7: Trajectory error based on the camera frame: X-axis of tag frame (a), Y-axis of tag frame (b), Z-axis of tag frame (c), ϕ of the tag frame (d)

6. Conclusion

This paper presented an SMC navigation system, which worked by the combination of fuzzy logic system, model reference approach, and tag-based fiducial marker detection to maneuver the drone in the indoor environment. The pa-

rameters of SMC were determined by fuzzy logic system and model reference approach. The desired set-points of the control system were obtained by AprilTag. The results represented the satisfactory performance of the SMC to navigate the drone from home to the target point. In addition, it demonstrated higher accuracy and reliable performance of the algorithms to accomplish various designed trajectories.

While the proposed method demonstrates efficiency, there are certain limitations to consider. One such limitation is that the tag marker must remain within the camera's field of view for the drone to track the desired trajectory. In future endeavors, it is suggested to explore intelligent algorithms that can determine the desired trajectory, representing the minimal path to the target while avoiding obstacles. This enhancement could contribute to a more versatile and robust navigation system.

References

[1] J. Shahmoradi, E. Talebi, P. Roghanchi, and M. Hassanalian: A comprehensive review of applications of drone technology in the mining industry. *Drones*, **4**(3), (2020), 1–25, DOI: 10.3390/drones4030034.

[2] J.R. Cauchard, A. Tamkin, C.Y. Wang, L. Vink, M. Park, T. Fang, and J.A. Landay: Drone.io: A gestural and visual interface for human-drone interaction. *14th ACM/IEEE International Conference on Human-Robot Interaction (HRI)*, (2019), 153–162. DOI: 10.1109/HRI.2019.8673011

[3] R. Casado and A. Bermúdez: A simulation framework for developing autonomous drone navigation systems rafael. *Electronics*, **10**(1), (2021), 1–7. DOI: 10.3390/electronics10010007

[4] G. Macrina, L.D.P. Pugliese, F. Guerriero, and G. Laporte: Drone-aided routing: A literature review. *Transportation Research Part C: Emerging Technologies*, **120** (2020), 102762. DOI: 10.1016/0003-4916(63)90068-X

[5] B. Selma, S. Chouraqui, and H. Abouaïssa: Fuzzy swarm trajectory tracking control of unmanned aerial vehicle. *Journal of Computational Design and Engineering*, **7**(4), (2020), 435–447. DOI: 10.1093/jcde/qwaa036

[6] L. Cedro and K. Wieczorkowski: Optimizing pid controller gains to model the performance of a quadcopter, *Transportation Research Procedia*, **40** (2019), 156–169. DOI: 10.1016/j.trpro.2019.07.026

[7] T.T. Mac, C. Copot, T.T. Duc, and R.D. Keyser: Ar.drone uav control parameters tuning based on particle swarm optimization algorithm. IEEE International Conference on Automation, Quality and Testing, *Robotics (AQTR)*, (2016), 1–6. DOI: 10.1109/AQTR.2016.7501380

[8] V.M. Babu, K. Das: and S. Kumar: Designing of self tuning pid controller for ar drone quadrotor. *18th International Conference on Advanced Robotics, ICAR* (2017), 167–172. DOI: 10.1109/ICAR.2017.8023513

[9] A.R. Merheb, H. Noura, and F. Bateman: Emergency control of ar drone quadrotor uav suffering a total loss of one rotor. *IEEE/ASME Transactions on Mechatronics*, **22**(2), (2017), 961–971. DOI: 10.1109/TMECH.2017.2652399

[10] A. Sagitov, K. Shabalina, L. Sabirova, H. Li, and E. Magid: ARTag, AprilTag and CALTag Fiducial Marker Systems: Comparison in a Presence of Partial Marker Occlusion and Rotation. *Proceedings of the 14th International Conference on Informatics in Control, Automation and Robotics*, **2** (2017), 182–191. DOI: 10.5220/0006478901820191

[11] I. Azmi, M.F. Nasrudin, N.S. Sani, and A.H.A. Rahman: ArUcoRSV: Robot Localisation Using Artificial Marker, Robot Intelligence Technology and Applications. RiTA 2018. *Communications in Computer and Information Science*, **1015** (2019), 189–198. DOI: 10.1007/978-981-13-7780-8_15

[12] S. Kawabata, J.H. Lee, and S. Okamoto: Obstacle avoidance navigation using horizontal movement for a drone flying in indoor environment. *3rd International Conference on Control, Artificial Intelligence, Robotics and Optimization, ICCAIRO* (2019), 1–6. DOI: 10.1109/ICCAIRO47923.2019.00009

[13] D. Malyuta, C. Brommer, D. Hentzen, T. Stastny, R. Siegwart, and B. Roland: Long-duration fully autonomous operation of rotorcraft unmanned aerial systems for remote-sensing data acquisition. *Journal of Field Robotics*, **37**(1), (2020), 137–157. DOI: 10.1002/rob.21898

[14] D. Tang, T. Hu, L. Shen, Z. Ma, and C. Pan: Apriltag array-aided extrinsic calibration of camera–laser multi-sensor system. *Robotics and Biomimetics*, **3**(1), (2016). DOI: 10.1186/s40638-016-0044-0

[15] M. Gheisarnejad and M.H. Khooban: An intelligent non-integer PID controller-based deep reinforcement learning: Implementation and experimental results. *IEEE Transactions on Industrial Electronics*, **68**(4), (2021), 3609–3618. DOI: 10.1109/TIE.2020.2979561

[16] N. Merayo, D. Juarez, J.C. Aguado, I. de Miguel, R.J. Durán, P. Fernández, R.M. Lorenzo, and E.J. Abril: PID Controller Based on a Self-Adaptive Neural Network to Ensure QoS Bandwidth Requirements in Passive Optical Networks. *Journal of Optical Communications and Networking*, **9**(5), (2017), 433. DOI: 10.1364/JOCN.9.000433

[17] D. Wang, M. Wang, and Y. Li: Genetic and fuzzy fusion algorithm for coal-feeding optimal control of coal-fired power plant. *International Symposium on Computer, Consumer and Control*, 1, (2020), 500–503. DOI: 10.1109/IS3C50286.2020.00136

[18] M. Navabi and M. RajabAliFardi: Quaternion based fuzzy gain scheduled pd law for spacecraft attitude control. *6th Iranian Joint Congress on Fuzzy and Intelligent Systems, CFIS*, **2018**(3), (2018), 149–151. DOI: 10.1109/CFIS.2018.8336660

[19] W. Salabun, J. Więckowski, A. Shekhovtsov, K. Palczewski, S. Jaszczak, and J. Wątróbski: How to apply fuzzy miso pid in the industry an empirical study case on simulation of crane relocating containers. *Electronics*, **9**(12), (2020), 1–15. DOI: 10.3390/electronics9122017

[20] J.Z. Shi: A Fractional Order General Type-2 Fuzzy PID Controller Design Algorithm. *IEEE Access*, **8** (2020), 52151–52172. DOI: 10.1109/ACCESS.2020.2980686

[21] Z. Han, Z. Liu, L. Kong, L. Ding, J.-W. Wang, and W. He: Adaptive fuzzy control for a hybrid spacecraft system with spatial motion and communication constraints. *IEEE Transactions on Fuzzy Systems*, **30**(8), (2022), 3247–3256. DOI: 10.1109/TFUZZ.2021.3111442

[22] M.S. Amiri and R. Ramli: Visual navigation system for autonomous drone using fiducial marker detection. *International Journal of Advanced Computer Science and Applications (IJACSA)*, **13**(9), (2022), 683–690. DOI: 10.14569/IJACSA.2022.0130981

[23] J.A. Abd, M.A. Hannan, A. Mohamed, and M.G.M. Abdolrasol: Fuzzy logic speed controller optimization approach for induction motor drive using backtracking search algorithm. *Measurement*, **78**, (2016), 49–62. DOI: 10.1016/j.measurement.2015.09.038

[24] M.S. Amiri, R. Ramli, and N. Aliman: Adaptive swarm fuzzy logic controller of multi-joint lower limb assistive robot, *Machines*, **10**(6), (2022), 425, DOI: 10.3390/machines10060425

[25] N. Aliman, R. Ramli, S. Mohamed Haris, M.S. Amiri, and M. Van: A robust adaptive-fuzzy-proportional-derivative controller for a rehabilitation lower limb exoskeleton. *Engineering Science and Technology, an International Journal*, **35** (2022), 101097. DOI: 10.1016/j.jestch.2022.101097

[26] M.S. Amiri and R. Ramli: Intelligent trajectory tracking behavior of a multi-joint robotic arm via genetic – swarm optimization for the inverse kinematic solution. *Sensors*, **21**(9), (2021), 3171. DOI: 10.3390/s21093171

[27] M.S. Amiri, R. Ramli, and A.H. Faizal: Simultaneous localization and mapping and tag-based navigation for unmanned aerial vehicles. *International Journal of Integrated Engineering*, **15**(5), (2023), 225–232. DOI: 10.30880/ijie.2023.15.05.024

[28] K.A. Juhari, R. Ramli, S.M. Haris, Z. Ibrahim, and A.Z. Mohamed: Development of Floor Mapping Mobile Robot Algorithm Using Enhanced Artificial Neuro-Based SLAM (ANBS). *Jurnal Kejuruteraan*, **3**(1), (2020), 59–64. DOI: 10.17576/jkukm-2020-si3(1)-09